Experiments in Fluids (2005) 38: 476–484
DOI 10.1007/s00348-005-0928-1

ORIGINALS

A. Stocchino · M. Guala

Particle-wall collision in shear thinning fluids

Received: 18 June 2004 / Revised: 22 December 2004 / Accepted: 23 December 2004 / Published online: 25 February 2005

Abstract The present study deals with the measurements of the impact w_i and rebound w_r velocities of steel particles in different fluids colliding with a rigid wall. The results are presented in terms of the coefficient of restitution $e = w_r/w_i$ as a function of the Stokes number (ratio between the particle inertia and the viscous forces). We focus the attention on possible differences between rebounds that occur in Newtonian fluids and in non-Newtonian, shear thinning fluids. The measurements of wet coefficients of restitution in Newtonian fluid are in good agreement with the experimental data found by Gondret et al. (2002). In the range of Stokes number investigated, an increase of the coefficient of restitution with the shear thinning fluid is clearly observed with respect to the Newtonian data. Particular attention has been dedicated to techniques of image processing to perform an optimal estimation of the particle centroid in highly noisy images.

1 Introduction

Many natural phenomena as well as many applications in mechanical engineering involve particle–particle or particle–wall collisions. Understanding of the mechanics of a single collision is an essential input in modeling natural or industrial processes such as, among others, agglomeration, granular flows, sediment transport and, in general, any multi-phase flow problems where solid particles are involved.

During recent decades, a considerable effort has been dedicated to study the dynamics of collisions in terms of the coefficient of restitution e, defined as the ratio of the moduli of the rebound (w_r) and the impact (w_I) velocity. The coefficient of restitution is commonly adopted to model both the collision between two particles and the collision between one particle and a wall and, therefore, it can be inserted as an input into more complicated mechanical models. The case of dry collisions, i.e., when a particle collides with a rigid wall falling in fluids with negligible dynamic viscosity (e.g., air), has been extensively studied in the past. Starting from the classical Hertzian theory, which is based on the hypothesis of a perfectly elastic rebound and eventually predicts a coefficient of restitution equal to unity, many studies have been devoted to understand the non-ideal rebounds, including different sources of energy loss that cause a decrease of the dry coefficient of restitution. Along this line, the value of the coefficient of restitution is found to be influenced by plastic deformation (Johnson 1985), waves and vibrations (Zener 1941; Hunter 1957; Sondergaard et al. 1990), and viscoelasticity (Falcon et al. 1998). Sondergaard et al. (1990) have investigated experimentally the influence of the ratio of the particle diameter D and the plate thickness b, showing a decrease of e with increasing D/b. Moreover the authors studied the dependence of e on the position of the plate supports and on the impact velocity. The latter aspect has also been studied in detail by Falcon et al. (1998) where successive rebounds have been measured showing a decrease of e with the impact velocity.

When a particle–wall collision occurs inside a viscous fluid, viscous dissipation has to be taken into account. The effect of a Newtonian fluid has been extensively studied both theoretically and experimentally. Davis et al. (1986) solved the coupled problem of the lubrication layer together with solid deformation showing that the particle–wall collision is described by the Stokes number defined as:

A. Stocchino (✉)
Dipartimento di Ingegneria Ambientale,
Università di Genova, via Montallegro 1,
Genova, Italy
E-mail: jorma@diam.unige.it

M. Guala
Institute of Hydromechanics and Water
Resources Management, ETH Zurich,
Zurich, Switzerland

$$\mathrm{St} = \frac{2mw_\mathrm{i}}{3\pi\mu D^2} = \frac{1}{9}\frac{\rho_\mathrm{P}}{\rho_\mathrm{f}}\mathrm{Re} \quad \mathrm{Re} = \rho_\mathrm{f} = \frac{Dw_\mathrm{i}}{\mu} \tag{1}$$

where D is the diameter of the spherical particle, ρ_P and ρ_f are the particle and fluid densities respectively, m is the particle mass, μ is the fluid dynamic viscosity, and Re is the particle Reynolds number. The elasticity parameter is given by:

$$\varepsilon = \frac{\theta\mu w_\mathrm{i} D^{3/2}}{8z_0^{5/2}} \tag{2}$$

where z_0 is the distance between the two approaching surfaces at which the velocity assumes the values w_i, $\theta = (1-v_1^2)/\pi\, E_1 + (1-v_2^2)/\pi\, E_2$ and v_1,v_2 and E_1,E_2 are the Poisson's ratio and Young's modulus of elasticity for the ball and the wall, respectively. They also found a critical value of the Stokes number below which no rebound occurs that weakly depends on the elasticity parameter. The dependence of the coefficient of restitution on the Stokes number has been experimentally verified in many studies (Barnocky and Davis 1988; Lundberg and Shen 1992; Zenit and Hunt 1998, 1999; Gondret et al. 1999, 2002; Joseph et al. 2001; Davis et al. 2002), together with other aspects of collision dynamics. For example, Joseph et al. (2001) with a pendulum experiment investigated a possible role of the particle roughness, while Gondret et al. (2002) analyzed the entire trajectory of the colliding particle.

All the experiments mentioned regard the influence of a Newtonian fluid. The main purpose of the present experiments is to study whether the properties of a shear thinning fluid may influence the measured coefficient of restitution. So far, many works are available in the literature regarding the settling of a solid particle in non-Newtonian fluids (e.g., Mena et al. 1987; Becker and McKinley 1994; Navez and Walters 1996; Bot et al. 1998). The latter works are mainly focused on the effect of the rheological properties of the fluid, e.g., visco-elasticity, on the dynamics of the particle motion. In the cited works, shear thinning fluids have been used for the experiments, which in most cases are described by a power law model as the Ostwald-de-Waele equation. To our knowledge, no experiments have been performed to study the coefficient of restitution with a particle immersed in a shear thinning fluid.

To measure the coefficient of restitution starting from recorded images, we developed a new digital method to evaluate the position of the centroid of the falling particle. The proposed method is specifically designed to treat very noisy images.

The rest of the paper proceeds as follows. The experimental set up and the working fluids are described in the next section. Then, the image analysis method is discussed in detail. The experimental results are first presented for the coefficient of restitution obtained with a Newtonian fluid and then the measurements with the shear thinning fluid are compared with the Newtonian case. Some brief conclusions follow.

Table 1 Experimental parameters: particle properties

No.	D (mm)	ρ (g/cm^3)	m (g)	E (GPa)	v
1	15.584	8.109	16.0698	210	0.30
2	15.278	8.112	15.1469	210	0.30
3	13.994	7.702	11.0520	190	0.27
4	10.977	8.105	5.6128	210	0.30

1.1 Experimental apparatus and rheological properties of the working fluids

The experiments were carried out in a cubic Perspex tank with lateral size of 50 cm and a glass bottom 2.5 cm thick. The Young's modulus of the bottom wall is 60 GPa and the Poisson's ratio is 0.23. Different spherical Nickel-steel particles were released by means of an electromagnetic device located approximately 15 cm above the bottom of the tank. The main parameters of the spherical particles are shown in Table 1. In the present experiments the influence of the elastic properties of the material has not been studied. The entire experimental setup is shown in Fig. 1.

The dimensions of the experimental tank are such to avoid any influence of the side walls; the distance of the walls from the impact being much larger than the critical distance predicted by Sondergaard et al. (1990). Moreover, the diameters of the spherical particles used in the present work are sufficiently large to consider the surface forces negligible during the rebound. The release mechanism imposed some limitations in the choice of the materials for the particles, which must be made of ferromagnetic material. Therefore, it was impossible to drop less dense particles (plastic or glass spheres).

Regarding the working fluids, measurements of the immersed coefficient of restitution with Newtonian fluids were performed using aqueous solutions of Glycerol. Solutions were produced starting from a Glycerol 98% pure and adding different volumes of distilled water obtaining twenty different mixtures. Dynamic viscosities of Glycerol solutions were measured using a Haake falling ball viscometer and ranged from 0.825 mPa s for clear distilled water, up to 468.04 mPa s for a 98% aqueous solution of Glycerol at a temperature of about 20 °C.

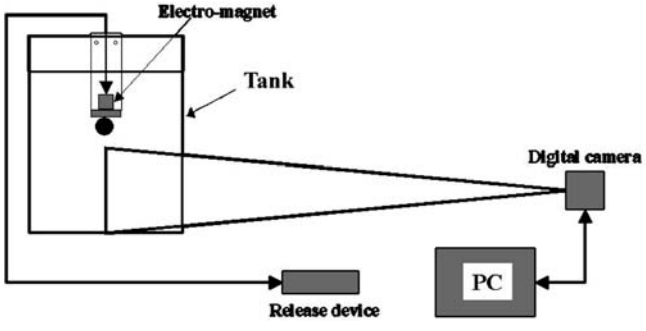

Fig. 1 Sketch of the experimental apparatus

The shear thinning fluid used in the present experiments was an aqueous solution of carboxymethyl cellulose (CMC). CMC has a very wide range of applications, for example, in detergents and soaps it acts as a soil-suspended agent, in food products it is used for its properties of thickener, water binder and emulsion stabilizer. CMC semisynthetic white granules are colorless and odorless and are classified as a nontoxic water soluble polymer, which is available at various levels of viscosity. It is the sodium salt of CMC (CH_2COONa) that promotes water solubility, which is not affected by the temperature of the water itself. The resulting solutions of CMC are transparent to light. However, increasing the concentration of the transparency decreases rapidly, worsening the optical characteristics of the solution in terms of absorption and diffusion of light.

One of the most important properties of CMC is the viscosity building character. Each polymer chain of diluted solution of CMC is hydrated and extended and exhibits a stable viscosity. Regarding the rheological behavior of CMC solutions, they can be both pseudoplastic and thixotropic depending on the type and the time scale of the process under investigation. However, almost all types of CMC are strongly pseudoplastic. The latter property is the main reason for having chosen CMC solutions as a shear thinning fluid for the present experiments, together with sufficiently good optical properties. The rheological properties of CMC have been widely studied in the last decade for both low and high concentrations (Young and Shoemaker 2001; Kokini and Surmay 1994; Ghanam and Esmail 1997; Escudier and Presti 1999; Barbesta et al. 2001; Edali et al. 2001). The rheological response to steady-state shear flow tests for the CMC can be modeled by the power law Ostwald-de-Waele equation written as (Ghanam and Esmail 1997; Edali et al. 2001):

$$\tau = k\gamma^n, \tag{3}$$

where τ is the shear stress (Pa), k is the consistency index (Pa s^n), γ is the shear rate and the exponent n is the flow behavior index, which assumes values less than unity.

Table 2 shows the values of both k and n for the solutions used during the present experiments. The data reported in Table 2 have been obtained from rheological tests performed using the Haake-Rheostress RS100 system. The above system features two test modes, namely the controlled rate mode (CR) and an oscillating test mode (OSC). The parameters of the Ostwald-de-Waele equation were obtained assigning a shear rate in the CR mode. The RS100 allows for the measurements of very low values of strain or shear rate due to its high encoder resolution. The present rheological tests agree fairly well with previous experiments (Ghanam and Esmail 1997; Edali et al. 2001). Test values of the apparent viscosity η, defined as the ratio between the shear stress and the shear rate τ/γ, were also obtained. In Fig. 2 the dependence of the viscosity on the shear rate is shown for all the solutions of CMC used. The viscosity η decreases for increasing shear rate, though extremely slowly for high values of γ.

Table 2 Ostwald-de-Waele equation constants of CMC solutions. Concentrations are expressed in terms of volume fraction

CMC (%)	k (Pa s^n)	n
0.49751	0.0396	0.9457
0.63425	0.0483	0.9309
0.70922	0.0538	0.9227
0.80429	0.0617	0.9123
0.90091	0.0708	0.9018
0.92879	0.0737	0.8987
1.06007	0.0889	0.8844
1.23457	0.1142	0.8654

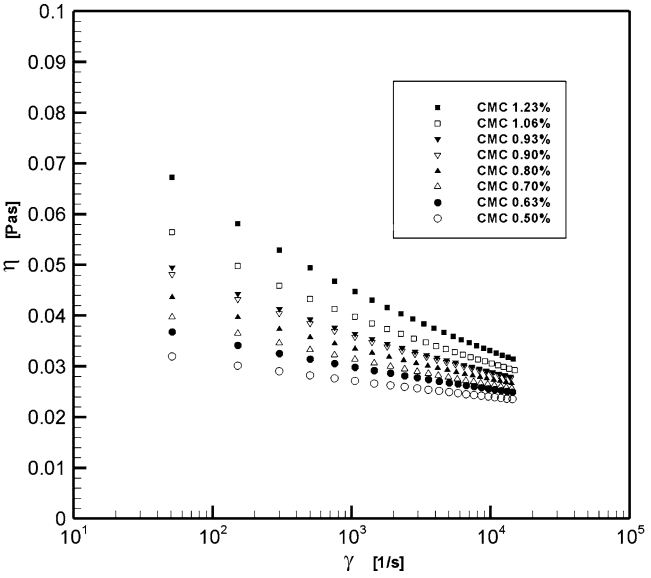

Fig. 2 Viscosity versus shear rate of CMC solutions

The motion of the falling ball was recorded using a high-speed digital camera with an acquisition rate of 500 Hz and an image resolution of 320×280 pixel. Finally, note that relatively low concentrations of CMC were used, due to the poor transparency of high concentration solutions, which may cause the falling ball to be almost invisible in the recorded images.

2 Digital image evaluation method

In the present section we describe how digital images were elaborated to obtain the particle position in each frame and, eventually, the estimate of the coefficient of restitution. We also suggest a novel method of analysis, suitable for highly noisy images, derived from classical digital particle image velocimetry evaluation methods. In order to increase the contrast, each digital image, originally in gray scale color mode, is binarized by selecting the threshold value which best separates the sphere from the background. Once the image has been binarized, a standard algorithm to locate the particle

centroid is based on the geometrical definition of the centroid. The latter procedure is often successfully used in experimental measurements of particle trajectories (Becker and McKinley 1994; Kharaz et al. 1999; Gorham and Kharaz 2000, 2001; Joseph et al. 2001; Gondret et al. 2002). However, the image area used during the evaluation of the centroid position is prescribed once a threshold value is set, which is not always a straightforward procedure. In fact, during the acquisition of the digital frames many unexpected drawbacks may occur to deteriorate the quality of the image. In case of uneven lighting of the tank or reflections, the shape of the recorded particle image may not be circular.

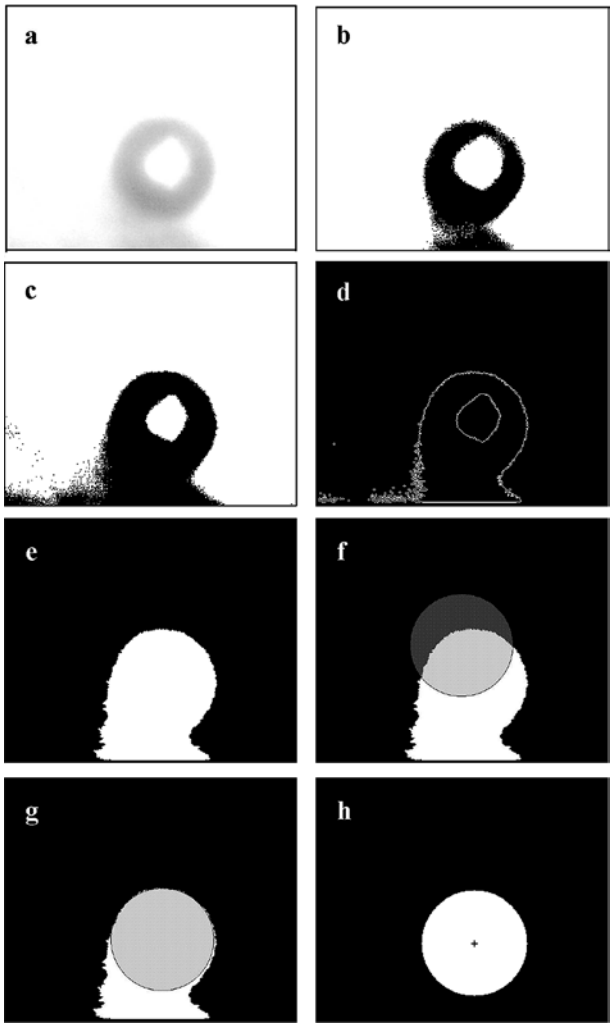

Fig. 3 Sequence of images illustrating the steps of the proposed algorithm. **a** Original gray scale image of an experiment in CMC, which shows how the poor optical characteristic of the fluid can produce a very noisy image. **b** Binarized image obtained with a high threshold value. **c** Binarized image obtained with a low threshold value. **d** *Edge* image after the edge detection algorithm. **e** Image of the object identified as the particle. **f** Superposition of the fictitious particle (*gray circle*) placed in the center of the image and image **e**. **g** Best overlap after the cross correlation analysis. **h** Image of the final particle image obtained by the algorithm with the location of the centroid (+). Note that in **d–h** the *colors* are inverted

Thus, the shape of the binarized particle image may change depending on the value of the threshold and eventually the location of the centroid can be affected (Kharaz et al. 1999). Unfortunately, a simple threshold operation is unable to remove reflections on the particle image, see for example Fig. 3a–c.

Hence, particle position measurements based on the geometrical definition of centroid become threshold dependent, the latter being a user defined parameter (Kharaz et al. 1999; Gorham and Kharaz 2000, 2001).

An alternative approach to the measurements of the particle position is based on edge detection and clustering methods. Different methods have already been applied in experimental applications, e.g., particle trajectories tracking during a collision (Labous et al. 1997) or in particle image velocimetry experiments of multiphase flows (Khalitov and Longmire 2002). The main aspect of these techniques is that particles are extracted from the entire image and labeled as single objects and then the centroid is evaluated for the single object. Although the method suggested by Labous et al. (1997) is able to solve part of the problems related to the background noise and the uneven illumination, results still strongly depend on the size and shape of the objects detected in the image. In fact, the position of the object (particle) is still evaluated in terms of the geometric centroid.

In the present experiments we work with aqueous solutions of Glycerol and CMC that have an acceptable clearness only for low concentrations (see Fig. 4). For increasing Glycerol and, especially, CMC concentration both the transparency of the optical medium and the light diffusion are seriously affected. In fact, the particle and its shadow near the bottom wall are often recorded with a similar gray intensity, for example see Fig. 3a . Hence, the size and shape of the particle image may not be well-defined and an algorithm to locate the centroid, based on its geometrical definition, produces poor results. Based on these observations, we formulated a new method to measure the position of a particle which is reasonably independent of the threshold value. We briefly summarize the main steps of the algorithm.

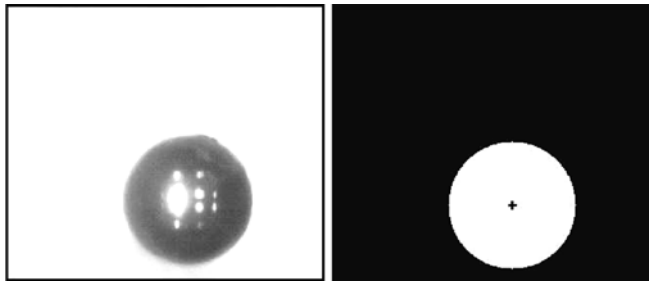

Fig. 4 *Left*: example of a high-quality image recorded during a low concentration Glycerol experiment. *Right*: the same image after processing, the symbol (+) indicates the position of the centroid evaluated with its geometrical definition

Starting from the original gray scale image, a threshold is automatically applied based on the intensity histogram. The threshold value is such to contain the entire particle, even though the resulting binarized image is noisy. Figure 3b, c shows the difference between a high threshold image, where part of the particle is lost, and a low threshold image, where the noise is higher but the whole particle is preserved. The second step is to apply an edge detection algorithm. We used a differentiation-based edge detection method, which locates an edge finding all zero-crossings of the image intensity Laplacian. The *edge* image obtained after processing is shown in Fig. 3d; note that the colors have been inverted just to illustrate each step of the algorithm more clearly. When all the edge points are identified, they have to be linked into closed chains that correspond to single objects in the image. Any pixel inside each linked-edge belongs to that object and its intensity is set equal to the edge points. After these procedures we are left with a finite number of *white* objects on a *black* background. We then clean up the image using a procedure based on the size of each single object in terms of the number of pixels. The object identified as the moving particle must have the largest size. Finally, the result of this object detection algorithm is shown in Fig. 3e, where only one object (the sphere) is left. The novel aspect of the method herein suggested, regards the procedure employed to estimate the position of the particle. From Fig. 3e it is clear that using a simple geometrical definition for the centroid would yield unacceptable results. However, the shape of the original particle is still preserved, except for a region close to the bottom of the image. This means that a matching between a fictitious target object, representing the image of the real sphere, inserted into the image plane, and the recorded object Fig. 3e could be easily found. To perform this image matching, we implement a cross-correlation analysis, which is a fundamental tool for particle image velocimetry measurements (Raffel et al. 1998). We prepare an artificial image of the same size with a fictitious circle with the same dimensions, in pixel, of the real particle placed in the center of the image plane. Note that the knowledge of the exact dimensions of the particle is not strictly necessary. Figure 3f shows the fictitious particle superimposed on the recorded particle image. We then perform a two-dimensional cross-correlation via FFT between the artificial image and the recorded image, providing the best matching between the two objects with subpixel accuracy. In fact, the displacement of the correlation peak in the correlation plane is the distance covered by the fictitious particle from the starting position (center of the image plane). Therefore, we can infer the position of the real sphere from the centroid of the fictitious particle. Figure 3g shows the matching of the objects and Fig. 3h shows the centroid of the sphere (black cross in the figure). The proposed method has the advantage of being independent of the threshold value and, as a consequence, of the shape and size of the particle image; and even if the recorded image is highly noisy the results are accurate. The method has been

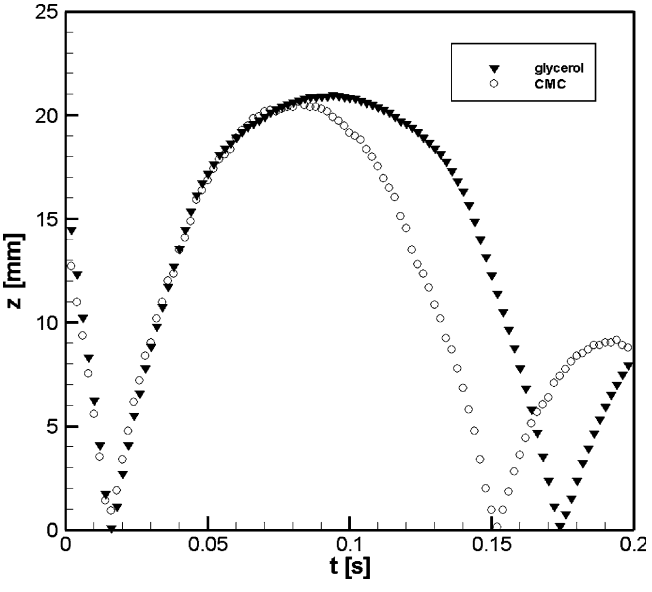

Fig. 5 Example of a complete particle trajectory. The *filled symbols* correspond to an experiment performed with ball 3 released with a solution of Glycerol (60%). *Hollow circles* correspond to an experiment performed with ball 3 released with a solution of CMC (1.23457%)

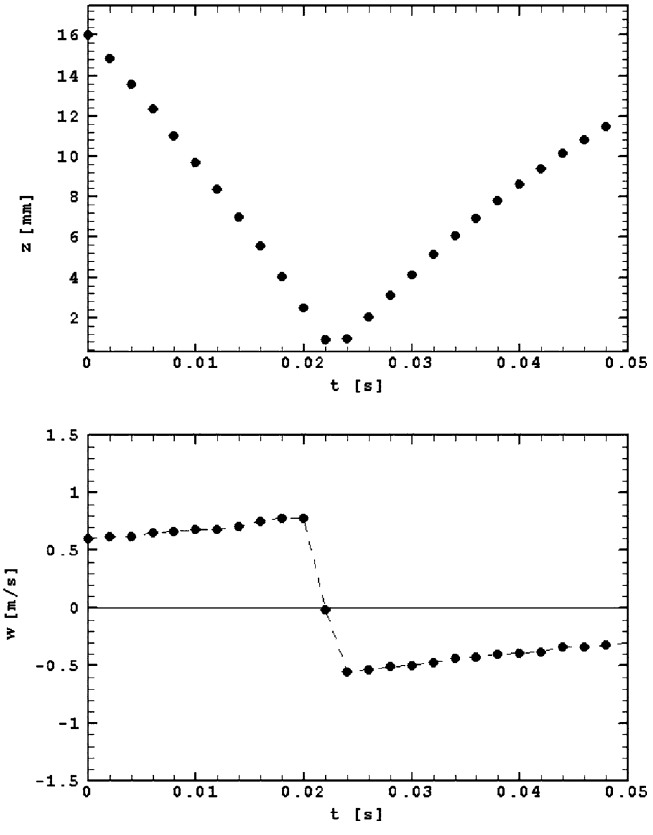

Fig. 6 Particle trajectory and velocity during the first collision for an experiment with 1% solution of CMC and ball 1

tested using high-quality images like the one shown in Fig. 4.

3 Velocity estimation and error analysis

Once the position of the particle is found in all images, the trajectory of the sphere is known. Examples of particle trajectory and velocity are reported in Figs. 5 and 6. Starting from the trajectory, a least square linear fitting over a proper number of points before and after the rebound is used to calculate the coefficient of restitution, since the slopes of the fitted lines represent the rebound and impact velocities. The linear fitting of the trajectories near the rebound has been often used in particle wall collision experiments (see e.g., Joseph et al. 2001; Davis et al. 2002; Gondret et al. 2002). The number of points used in the fitting is crucial for the final result, since a small error in the determination of the slopes of the fitting lines may cause a large error in terms of the coefficient of restitution. Following Joseph et al. (2001), we used five–ten points performing an iterative fitting maximizing the linear correlation coefficient of the fitted line to the experimental data, imposing a minimum acceptable value of 0.99.

Considering the single particle image, the particle dimension in terms of pixels ranges between 100 and 140. The precision of the position could be estimated within an error ranging from 0.37% to 0.50% of the particle diameter, which implies an absolute error of 0.055 mm regardless of the subpixel accuracy for the correlation peak detection. Introducing the latter refinement in the image processing, we expect that the error will be likely reduced by half. We then estimate the standard deviation of the particle position of each trajectory with respect to the fitting line obtaining a most probable value of 0.033 mm. This value is consistent with the expected error discussed above. In terms of particle velocity the error distribution is shown in Fig. 7. Finally, the error of the present measurements of the coefficient of restitution ranges from 1% to 6% depending on the impact velocity.

The velocity of the particle along its whole trajectory can be evaluated, starting from the discrete sampled position, using a first-order backward or forward differencing scheme, as shown in Fig 6. In agreement with Gondret et al. (2002), we do not observe a decrease in the velocity while the particle is approaching the wall as was found for the pendulum experiments (Joseph et al. 2001).

4 Results

In this section we present the measured coefficient of restitution e as a function of the Stokes number for both Newtonian and non-Newtonian fluids. The Stokes number is the pertinent nondimensional number in describing the dependence of the coefficient of restitution on the fluid and particle properties, as pointed out by Gondret et al. (2002). Our assumption is that this choice can be also fully justified for the case of the shear thinning fluid, provided an estimate for the proper viscosity to be used in its evaluation. In fact, for a non-Newtonian fluid the apparent viscosity η is a function of the rate of strain γ. The definition of the appropriate apparent viscosity is then crucial, since it controls the values of the impact Stokes number. Hence, while there is no ambiguity in the case of a Newtonian fluid, on the contrary, great care must be taken in providing a value

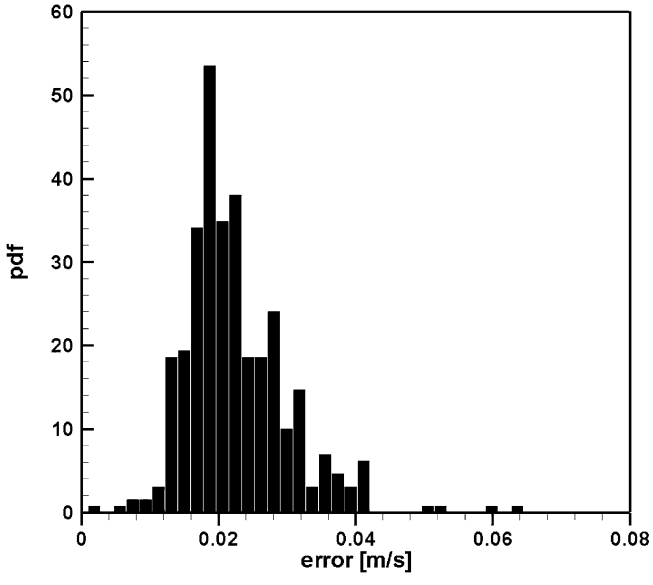

Fig. 7 Pdf of the error in estimating the particle velocity

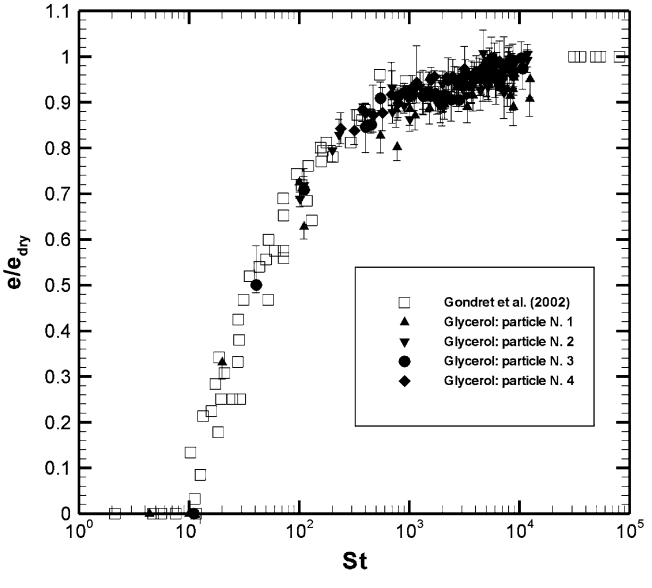

Fig. 8 Coefficient of restitution scaled with e_{dry} as a function of the impact Stokes number in the case of Newtonian fluid. The *hollow symbols* represents the measurements of Gondret et al. (2002)

for the apparent viscosity when a non-Newtonian fluid is studied.

4.1 Dry coefficient of restitution

We first measured the dry coefficient of restitution for the whole set of spherical particles to evaluate the influence of the ratio between the bottom plate thickness b and the particle diameter D. It is well known from previous experimental investigations that the coefficient of restitution of dry impact of spherical particles increases with the plate thickness until it is about four times the particle diameter (Zener 1941; Sondergaard et al. 1990), due to less vibrational losses related to flexural modes of the plates excited during the impact. Accordingly, we found a dry coefficient of $e_{\mathrm{dry}} = 0.91$, for particles 1 and 2, $e_{\mathrm{dry}} = 0.8$ for particle 3 and $e_{\mathrm{dry}} = 0.72$ for particle 4.

4.2 Wet coefficient of restitution: the Newtonian case

Figure 8 shows the measured immersed coefficient of restitution divided by the proper e_{dry} in the case of the Newtonian fluid as a function of the impact Stokes number. Moreover, in the same plot are reported the experimental data by Gondret et al. (2002), which were obtained with a similar experimental set up. The present measurements are in fairly good agreement with the cited data, reproducing all the main features of the particle collision dynamics. In particular, the normalized coefficients of restitution e/e_{dry}, for the range of Stokes number investigated, follow a clear trend described theoretically by Davis et al. (1986). The value of the critical Stokes number measured in the present experiments is around 10, which is in agreement with the observations of Gondret et al. (2002) and Joseph et al. (2001). No further comments are needed regarding the measurements of the immersed coefficient of restitution in the case of Newtonian fluid, since the present results do not add any new information with respect to previous studies. However, the measurements performed in Newtonian fluids had the purpose of both testing the image evaluation method described in Sect. 3 and, mainly, to allow for a methodologically rigorous comparison with the measurements in the case of the non-Newtonian fluid discussed in the next section.

4.3 Wet coefficient of restitution: the non-Newtonian case

In order to maintain the Stokes number as the pertinent dimensionless parameter to describe the behavior of the coefficient of restitution also with the shear thinning fluid, we should specify which is the proper viscosity to be used in calculating the Stokes number for each experiment. The viscosity, in the case of shear thinning fluids, is no longer a property of the fluid; instead, it depends on the local conditions of the flow expressed in terms of shear rate γ. An estimate of a typical shear rate can be made by selecting a characteristic velocity scale and a characteristic length scale. As a first attempt, we used the settling velocity W_s as a scale for the velocity and the particle diameter D as a typical length scale, obtaining a rate of strain equal to $W_{s/D}$. This choice is suitable to describe the particle settling dynamics, as reported in Mena et al. (1987), Becker and McKinley (1994), Navez and Walters (1996), and Bot et al. (1998), among others, and it is consistent with the analogous particle settling in Newtonian fluid. However, when the particle is approaching the wall, the representative rate of strain becomes higher, since the characteristic length scale is no longer the particle diameter, but the distance z between the two approaching surfaces. This may decrease to a value between z_0 and z_c, upper and lower boundaries, respectively, of the flow region where the lubrication approximation holds, as suggested in Joseph et al. (2001). Typical values of z_0 and z_c are $D/100$ and $D/10^5$, respectively (see Joseph et al. 2001). Moreover, the proper velocity scale was chosen as the impact velocity w_i, which in general could be different from the settling velocity W_s; therefore, a reasonable estimate of the shear rate in the case of a particle wall collision is found setting $\gamma = w_i/z_0$. As a consequence, the apparent viscosity consistent with the latter rate of strain drops down appreciably with respect to the value estimated using a rate of strain equal to $w_{I/D}$. Using the value suggested by Joseph et al. (2001) for z_0, the rate of strain at the impact is two orders of magnitude higher than the rate of strain while the particle is settling. The range of rate of strain estimated in the present experiments is between 1,380 s^{-1} and 11,000 s^{-1} and the measured

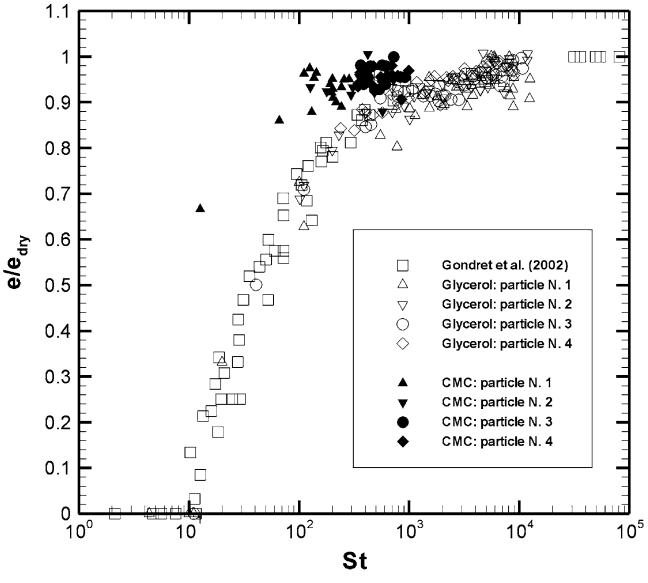

Fig. 9 Coefficient of restitution scaled with e_{dry} as a function of the impact Stokes number; comparison between the Newtonian measurements (*white* symbols) and non-Newtonian measurements (*black* symbols)

impact velocities range from 0.21 ms^{-1} to 1.3 ms^{-1}. The corresponding values of the viscosity η vary from 0.024 Pa s to 0.043 Pa s.

In Fig. 9a comparison of the coefficient of restitution observed with CMC against the data discussed in Sect. 5.2 is shown. In the range of Stokes number investigated in the present experiments, the coefficients of restitution for CMC solutions was observed to be higher compared to those obtained in Newtonian fluids, at a fixed Stokes number.

A possible explanation of this result may be found in the non-Newtonian rheological properties of the CMC. The shear thinning behavior of CMC solutions is taken into account through the correct determination of the viscosity and, therefore, of the Stokes number. This suggests that the increase of the coefficient of restitution of the CMC with respect to Newtonian fluids for a fixed value of the Stokes number has to be related to other rheological properties typical of the CMC. In particular, a possible role of the viscoelastic behavior of the CMC solutions is herein investigated. In many experimental works viscoelasticity and normal stresses have been extensively studied for aqueous solutions of CMC (Escudier and Presti 1999; Williamson et al. 1997; Windle and Beazley 1997; Barbesta et al. 2001), showing that in many flow regimes the order of magnitude of the normal stresses is comparable with the shear stress.

For a viscosity value ranging 10^{-2}–10^{0} Pa s, the lubrication approximation holds in a layer thickness of the order of 10^{-5}–10^{-3} m such that, for an impact velocity of order 1–0.1 ms^{-1}, a characteristic time scale of the order of 10^{-5}–10^{-2} s is given. This is in agreement with Joseph et al. (2001), since z_0 is assumed as $D/100 = 10^{-4}$ m. Then, assuming w_i/z_0 as a scale for γ we have corresponding to the lower viscosity a value for the shear rate $\gamma = 10^{3}$ s^{-1} and, corresponding to the higher viscosity, $\gamma = 10^{5}$ s^{-1} and, respectively, $\tau = 10^{2}$ and 10^{3} Pa. In the lubrication layer we have $\tau = \rho_f w_i^2$, thus varying only due to a variation of the impact velocity, regardless, at least indirectly, of viscosity. For the aqueous solution of CMC, with the apparent viscosity η of the order of 10^{-2} Pa s, the same criterion, although not fully appropriate for non-Newtonian fluids, yields to a time scale of the order of 10^{-5} s. The measured impact velocity in the non-Newtonian case allows for estimating $\tau = 10^{2}$–10^{3} Pa. For such high shear stress, or in other words high γ , it is possible that the effects of the normal stress $N_1(\gamma)$ are not negligible. It is reported in Kokini and Surmay (1994) for $\tau = 10^{-1}$–10 Pa and in Escudier and Presti (1999) for $\tau = 10^{2}$ that even for low CMC concentration (0.6% to 1.5% in volume) N_1 is of the same order of magnitude of τ. Precisely a dependence of the first normal stress on the shear stress is suggested in Escudier and Presti (1999) and reads:

$$N_1 = 0.85\tau^{1.25}. \tag{4}$$

Moreover, Williamson et al. (1997) provides an estimation of a characteristic relaxation time for some shear thinning fluids, which is expressed by:

$$\lambda = N_1(\gamma)/\left(2\eta\gamma^2\right). \tag{5}$$

Using Eq. 5 to estimate a relaxation time for the solutions used in the present experiments, it turns out that λ is of order $O(10^{-5})$, which is comparable with the time scale characteristic for particle-wall collisions as reported in Zenit and Hunt (1999), Joseph et al. (2001), and Gondret et al. (2002). This means that the fluid has enough time to experience such a viscoelastic effect while the particle is approaching the wall and expelling the fluid trapped in the particle wall gap, and it is thus able, in this short time, to provide a feed-back effect on the particle. Values of N_1 of the order of 10 Pa for τ of the order of 10^{3}–10^{4} Pa are also given in Windle and Beazley (1997), while in Barbesta et al. (2001) for the same τ, N_1 is of the order of 1–10 Pa.

The fact that shear thinning Newtonian fluids can react in a very short time providing, besides a shear stress, a normal stress in the presence of high velocity gradients, i.e. high shear rate, can be a possible explanation for the observed trends in our comparative analysis of the coefficients of restitution in Newtonian and non-Newtonian fluids.

5 Concluding remarks

The novel image evaluation method proposed yields accurate measurements of the particle position, even if the recorded image is highly noisy. When the noise affects the dimension and the shape of the particle image like in the present experimental measurements, the location of the centroid may not be accurate if a pure geometric algorithm is applied. Following the latter approach the final results are also strongly dependent on the threshold applied (Kharaz et al. 1999; Gorham and Kharaz 2000; Kharaz et al. 1999). In the literature, alternative methods based on edge detection and clustering methods can be found. However, the threshold value is still a user-defined parameter, which has to be tuned up in order to obtain reliable results (Labous et al. 1997). In the light of removing this dependence, we introduced mathematical tools commonly used in digital PIV analysis. As a consequence, the implementation of a two-dimensional cross correlation ensures that the results are almost completely independent from the threshold applied.

The main results on the coefficient of restitution may be summarized as follows: (1) the measurements performed in Newtonian fluids are in fairly good agreement with the data available in the literature, regarding both the overall trend as a function of the Stokes number and the value of the critical Stokes number; (2) the coefficient of restitution in the case of non-Newtonian fluids, for the range of Stokes number investigated, was observed to be higher compared to the Newtonian case; (3) the Stokes number remains the pertinent parameter even for

the shear thinning fluid provided a proper value for the viscosity, i.e., the value obtained using the shear rate related to the lubrication layer; and (4) the increase of the coefficient of restitution may be related to the non-negligible normal stresses, since the time scale associated with the particle rebound, within the lubrication layer, is long enough for the fluid to experience viscoelastic effects.

As a final comment, we acknowledge that the present experiments cover only a limited range of Stokes number in the case of non-Newtonian measurements. This was due to the non-perfect optical properties of the medium viscosity CMC used and to some limitations of the entire experimental set up (electromagnetic release device). As a consequence, the range of low Stokes number remains partially uncovered and the critical Stokes number could not be investigated. However, we expect that in the surroundings of the critical Stokes number viscoelastic effects may not be important since, in that case, the shear rate assumes a low value. We acknowledge also that possible effects of the surface roughness have not been considered in the present analysis, since particle roughness should play an important role only for values of the Stokes number less than a hundred, as described in Joseph et al. (2001). The behavior of the coefficient of restitution near the critical Stokes number remains an open question of particular interest and it will be the object of further experiments.

Acknowledgements The present research was supported by the Fondazione Cassa di Risparmio di Verona, Vicenza, Belluno and Ancona (RIMOF Project).

References

Barbesta F, Bousfield DW, Rigdahl M (2001) Modeling of rheological properties of coating colors. J Rheol 45(1):139–160

Barnocky G, Davis RH (1988) Elastohydrodynamic collision and rebound of spheres: experimental verification. Phys Fluids 31:1324–1329

Becker LE, McKinley GH (1994) The unsteady motion of a sphere in a viscoelastic fluid. J Rheol 38(2):377–403

Bot ETG, Hulsen MA, van den Brule BHAA (1998) The motion of two spheres falling along their line of centres in a Borger fluid. J Non-Newton Fluid 79:191–212

Davis RH, Serayssol JM, Hinch EJ (1986) The elastohydrodynamic collision of two spheres. J Fluid Mech 163:479–497

Davis RH, Rager DA, Good BT (2002) Elastohydrodynamic rebound of spheres from coated surfaces. J Fluid Mech 468:107–119

Edali M, Esmail MN, Vatistas GH (2001) Rheological properties of high concentrations of carboxymethyl cellulose solutions. J Appl Polym Sci 79:1787–1801

Escudier MP, Presti SS (1999) Drag reduction in the turbulent pipe flow of polymers. J Non-Newton Fluid 81:197–213

Falcon E, Laroche C, Fauve S, Coste C (1998) Behavior of one inelastic ball bouncing repeatedly off the ground. Eur Phys J B 3:45–57

Gondret P, Hallouin E, Lance M, Petit L (1999) Experiments on the motion of a solid sphere toward a wall: from viscous dissipation to elastohydrodynamic bouncing. Phys Fluids 11(9):2803–2805

Gondret P, Lance M, Petit L (2002) Bouncing motion of spherical particles in fluids. Phys Fluids 14(2):643–652

Gorham DA, Kharaz AH (2000) The measurement of particle rebound characteristics. Powder Technol 112:193–202

Gorham DA, Kharaz AH (2001) An experimental study of the elastic rebound of spheres. Powder Technol 120:281–291

Ghanam MT, Esmail MN (1997) Rheological properties of carboxymethyl cellulose. J Appl Polym Sci 64:289–301

Hunter SC (1957) Energy absorbed by elastic waves during impact. J Mech Phys Solids 5:162–171

Johnson KL (1985) Contact mechanics. Cambridge University Press, Cambridge

Joseph GG, Zenit JR, Hunt ML, Rosenwinkel AM (2001) Particle-wall collision in a viscous fluid. J Fluid Mech 433:329–346

Kharaz AH, Gorham DA, Salman AD (1999) Accurate measurement of particle rebound impact parameters. Meas Sci Technol 10:31–35

Khalitov DA, Longmire EK (2002) Simultaneous two-phase PIV by two-parameters phase discrimination. Exp Fluids 32:252–268

Kokini JL, Surmay K (1994) Steady shear viscosity first normal stress difference and recoverable strain in carboxymethyl cellulose, sodium alginare and guar gum. Carbohydr Polym 23:27–33

Labous L, Rosato AD, Dave RN (1997) Measurements of collisional properties of spheres using high-speed video analysis. Phys Rev E 56(5):5717–5725

Lundberg J, Shen HH (1992) Collisional restitution dependence on viscosity. J Eng Mech-ASCE 118(5):979–989

Mena B, Manero O, Leal LG (1987) The influence of rheological properties on the slow flow past spheres. J Non-Newton Fluid 26:247–275

Navez V, Walters K (1996) A note on settling in shear-thinning polymer solutions. J Non-Newton Fluid 67:325–334

Raffel M, Willert C, Kompenhans J (1998) Particle image velocimetry: a practical guide. Springer, Berlin Heidelberg New York

Sondergaard R, Chaney K, Brennen CE (1990) Measurements of solid spheres bouncing off flat plates. J Appl Mech-T ASME 57:694–699

Zener C (1941) The intrinsic inelasticity of large plates. Phys Rev 59:669–673

Zenit JR, Hunt ML (1998) The impulsive motion of a liquid resulting from a particle collision. J Fluid Mech 375:345–361

Zenit JR, Hunt ML (1999) Mechanics of immersed particle collisions. J Fluid Eng-T ASME 121:179–184

Williamson BP, Waletrs K, Bates TW, Coy RC, Milton AL (1997) The viscoelastic property of multigrade oils and their effect on journal bearing characteristics. J Non-Newton Fluid 73:115–126

Windle W, Beazley KM (1997) The role of viscoelasticity in blade coatings. Tappi J 51:340–348

Young SL, Shoemaker CF (2001) Measurements of shear-dependent intrinsic viscosities of carboxymethyl cellulose and xanthan gum suspensions. J Appl Polym Sci 42:2405–2408